Available online at www.sciencedirect.com
ScienceDirect
Ceramics International 35 (2009) 2545–2554
CERAMICS INTERNATIONAL
www.elsevier.com/locate/ceramint

Characteristic, cell response and apatite-induction ability of microarc oxidized TiO_2-based coating containing P on Ti6Al4V before and after chemical-treatment and dehydration

Daqing Wei [a,b,*], Yu Zhou [b], Chunhui Yang [a]

[a] School of Chemical Engineering and Technology, Harbin Institute of Technology, Harbin 150001, PR China
[b] School of Materials Science and Engineering, Harbin Institute of Technology, Harbin 150001, PR China

Received 13 October 2008; received in revised form 29 October 2008; accepted 29 December 2008
Available online 6 June 2009

Abstract

The structure, cell response and induction capability for apatite formation of the microarc oxidized (MAO) coating before and after chemical-treatment and subsequent dehydration at 400 °C were investigated. The surfaces of the chemically treated MAO (C-MAO) coatings before and after dehydration showed ribbon-like amorphous phase mainly containing Na, Ti and O elements with network morphology. Subsequent dehydration has no pronounced effect on the surface roughness, wetting ability, surface constituents and chemical state of Ti, Na and O of the C-MAO coating. The outer layers of the C-MAO coating before and after dehydration showed Na, Ti and O elements with uniform distributions along the surface depth. Chemical-treatment improves the apatite-forming ability of the MAO coating; however, subsequent dehydration greatly lowers that of the C-MAO coating, since it changed the ability of C-MAO coating to release Na^+ ions, which is unfavorable for the formation of Ti-OH groups. The apatite formed on the two coatings contained HPO_4^{2-} and CO_3^{2-} ions. In addition, the dehydration of the C-MAO coating seemed to be unsuitable for the cell proliferation on its surface.

Keywords: Coating; Titanium alloy; Microarc oxidation; Biomimetic apatite; Dehydration; MG63 cell

1. Introduction

Hydroxyapatite and bioactive glass–ceramic exhibit good bioactivity [1,2]. Unfortunately, these bioactive ceramic materials are not suitable for load-bearing conditions due to their poor mechanical properties [3,4]. Titanium and its alloys have been used extensively in skeletal repair and dental implants area because of their excellent toughness, mechanical strength, biocompatibility and corrosion resistance. However, titanium and its alloys exhibit poor bioactivity. To improve the bioactivity of titanium and its alloys, many surface modifying techniques, such as plasma spraying [5–7] and sol–gel method [8,9], have been developed to prepare bioactive coatings such as hydroxyapatite and calcium phosphate on titanium and its alloys. Plasma-sprayed HA coatings have been extensively investigated; however, when used in implants, they lack strength and reliability, as a result of the residual stress and partial decomposition of HA during the preparation process [6,10,11].

Titanium oxide (TiO_2) on titanium and its alloys have potential applications in biomedical regions [12,13]. Microarc oxidation (MAO) is a relatively convenient and effective technique to deposit ceramic coatings on the surfaces of titanium and its alloys [14]. Using this technique to deposit biocoatings on titanium and its alloys has received much attention in recent years [15–23]. However, most MAO TiO_2 coatings exhibit poor ability for apatite formation [16,20,24,25]. Hence, it is necessary to improve the apatite-forming ability of the MAO TiO_2 coatings for their biomedical applications [25,26].

Recently, a chemical etching (NaOH aqueous solution) has been developed to modify the surface of the MAO coating to improve its apatite-forming ability [27], and further investigation indicated that the chemically treated MAO (C-MAO)

* Corresponding author at: Institute for Advanced Ceramics, Harbin Institute of Technology, P.O. Box 3022#, Science Park, Yikuang Street, Harbin 150080, PR China. Tel.: +86 451 8640 2040 8511; fax: +86 451 8641 4291.
E-mail address: daqingwei@hit.edu.cn (D. Wei).

0272-8842/$36.00
doi:10.1016/j.ceramint.2008.12.014

coating is almost dehydrated after heat treatment at 400 °C. However, the structure, cell response and apatite-forming ability of the C-MAO coating after dehydration are not clear up to now. As reported, the formation of biomimetic apatite is highly dependent on the structure and composition of substrates [12,28]. In other words, the physical and chemical properties of the substrate surfaces have important influences on the induction capability for apatite formation of the substrates in a simulated body fluid (SBF), as well as the cell response. This study attempts to understand the effect of dehydration on the structure, cell response and SBF behaviors of the C-MAO coating.

2. Experimental data

2.1. Sample preparation

In the MAO experiment, Ti6Al4V plates (10 mm × 10 mm × 1.5 mm) were used as anodes and stainless steel plates were used as cathodes in an electrolytic bath. The Ti6Al4V plates were ground with 400, 600 and 800# SiC abrasive papers, ultrasonically washed with acetone and distilled water, and dried at 40 °C. A fresh electrolyte was prepared by dissolving reagent-grade chemicals of $(NaPO_3)_6$ (20 g/l) and NaOH (10 g/l) into deionized water for the MAO process. The applied voltage, frequency, duty cycle and oxidizing time were 300 V, 600 Hz, 8.0% and 5 min, respectively. The temperature of the electrolyte was kept at 40 °C by a cooling system. After the MAO treatment, each sample was treated in 10 mL NaOH aqueous solution with concentration of 5 mol/l at 60 °C for 24 h, and then gently washed with deionized water and dried at 25 °C. For dehydration, the C-MAO coating was heat-treated at 400 °C for 1 h with a heating rate of 10 °C/min and furnace cooling. The C-MAO coating after dehydration was labeled as CD-MAO.

The MAO coatings before and after treatment were incubated in 15 mL simulated body fluid (SBF) for 7, 14 and 28 days. Ionic concentrations of the SBF and human blood plasma are shown in Table 1, and the SBF was refreshed every other day. The SBF was prepared by dissolving reagent-grade chemicals of NaCl, $NaHCO_3$, KCl, $K_2HPO_4{\cdot}3H_2O$, $MgCl_2{\cdot}6H_2O$, $CaCl_2$, and Na_2SO_4 into deionized water and buffering at pH 7.40 with tris-hydroxymethyl-aminomethane ($(CH_2OH)_3CNH_2$) and 1.0 mol/l HCl at 37 °C [29].

Table 1
Ion concentrations of the SBF and human blood plasma.

Ion	Concentration (mmol/l)	
	SBF	Blood plasma
Na^+	142.0	142.0
K^+	5.0	5.0
Mg^{2+}	1.5	1.5
Ca^{2+}	2.5	2.5
Cl^-	147.8	103.8
HCO_3^{2-}	4.2	27
HPO_4^{2-}	1.0	1.0
SO_4^{2-}	0.5	0.5

2.2. Characterization

The surface phase compositions of the MAO, C-MAO and CD-MAO coatings before and after SBF incubation were analyzed by a glancing incidence X-ray diffraction (XRD, Philips X'Pert, Holland) using a Cu Kα radiation (40 kV, 35 mA). In the XRD experiment, the angle of the incident beam was fixed at 1° against the sample surfaces and the measurements were performed with a continuous scanning mode at a rate of 2°/min.

The surface characters of the samples were also depicted by an atomic force microscopy (AFM, DI.Bioscope, Veeco, USA) in an uncontacting tapping mode with curvature radius of 5–10 nm, resolution of *x*-, *y*-direction about 2 nm and *z*-direction about 0.5 nm and number of samples of 256. The average roughness (Ra) of the MAO and modified MAO coatings was calculated by analyses of AFM image.

Wetting angle was measured using the liquid drop method on a contact angle goniometer (CAM101, KSV Instruments Ltd, Finland).

Surface morphologies of the samples before and after SBF incubation were observed by a scanning electron microscopy (SEM, CamScan MX2600, CamScan Co., England). Before the SEM examination, the samples were coated a thin Au layer since the surfaces of the samples are not conductive. In addition, the surface constituents of the samples were detected by an energy dispersive X-ray spectrometer (EDS, Oxford Model 7537, England) equipped on the SEM system.

Changes in the atomic concentrations of Na, P, Ti and O with increasing depth near the surfaces of the C-MAO and CD-MAO coatings were analyzed by an Auger electron spectroscopy (AES) measurement performing with a Scanning Auger nanoprobe (PHI 700, ULVAC Inc., USA). The Auger electron take-off angle in the AES was 40° and the sample surfaces were sputtered by Ar^+ ions with a sputtering rate of 144 nm/min referencing SiO_2. The voltage and current intensity were 3 kV and 10 nA, respectively. The sputtered and analyzed areas on each surface were about 2 mm × 2 mm and 40 μm × 40 μm, respectively. The data acquisition was performed every 30 s.

An X-ray photoelectron spectroscopy (XPS, PHI 5700, American Physical Electronics) was used to detect the surface chemical compositions of the sample surfaces. An Al Kα (1486.6 eV) X-ray source with an anode power of 250 W (12.5 kV, 20 mA) was used to analyze the chemical state of Ti, Na, O, Ca, P, etc. with a hemispherical analyzer in a high-resolution mode. The XPS take-off angle was set at 45°. A region about 2 mm × 0.8 mm on each surface was analyzed. The measured binding energies were calibrated by the C1s (hydrocarbon C–C, C–H) of 285 eV.

Fourier transform infrared spectroscopy (FT-IR, Bruker Vector 22, Germany) was also used to analyze the structure of the MAO, C-MAO and CD-MAO coatings, as well as these coatings after SBF incubation for 28 days. In the FT-IR measurements, the resolution and scanning range were 4 and 4000–400 cm^{-1}, respectively.

Na concentrations of the SBF with incubation of all the coatings for 0–12 days were measured by an inductively

coupled plasma optical emission spectroscopy (ICP-OES, Optima 5300DV, Perkin-Elmer, USA). In the ICP-OES measurement, the ion concentrations of 10 mL SBF after immersion of each sample were measured. Two independent analyses were carried out for each solution.

The cell response of the samples was evaluated by preliminary in vitro MG63 cell tests. The pre-incubated cell lines were plated onto specimens with a cell density of 2×10^4 mL^{-1}, and then cultured in a humidified incubator with 5% CO_2 at 37 °C. Dulbecco's modified Eagle's medium (DMEM) with 10% fetal bovine serum (FBS) was used as the culturing medium. The proliferation behavior was determined by counting the number of cells after culturing them for 7 days. The cells were detached from the samples with 0.05% trypsin–EDTA and counted using a hemocytometer. To observe the morphology of the proliferated cells by SEM, the cultured samples were fixed by 4% paraformaldehyde for 20 min. The experimental data were represented as mean ± one standard deviation (SD) for $n = 5$. Statistical analysis was conducted via a one-way analysis of variance.

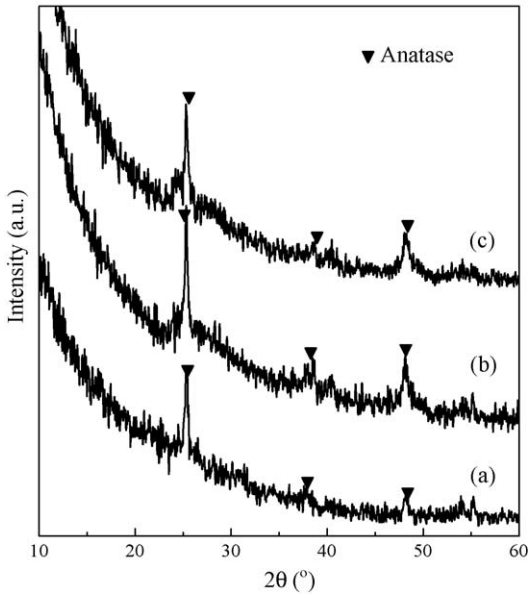

Fig. 1. XRD patterns of (a) MAO, (b) C-MAO and (c) CD-MAO coatings.

3. Results

3.1. Character of the C-MAO and CD-MAO coatings

Fig. 1 shows the XRD patterns of the surfaces of the MAO, C-MAO and CD-MAO coatings. All the coatings show the presence of anatase (Fig. 1a–c). However, besides diffraction peaks of anatase, new broad diffraction peaks at $2\theta = 22.5–35^\circ$ and 45–50° were observed on the surface of the CD-MAO coating (Fig. 1c), indicating the presence of amorphous phase, similar to the C-MAO coating (Fig. 1b).

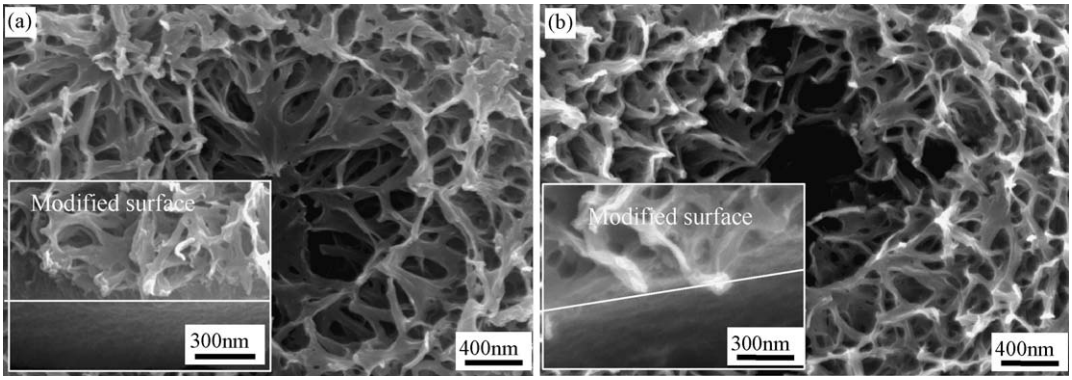

Fig. 2. Surface morphologies of (a) C-MAO and (b) CD-MAO coatings.

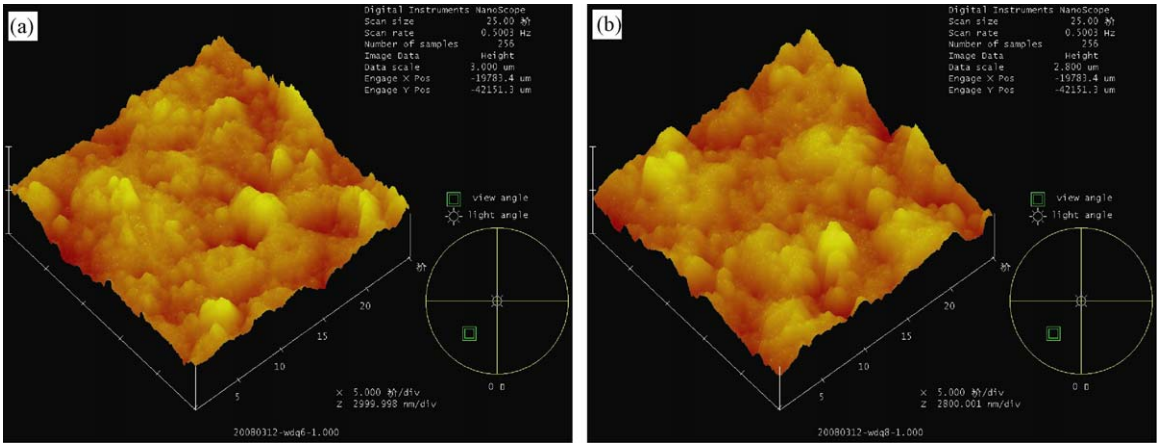

Fig. 3. The 3D AFM images of the surfaces of the (a) C-MAO and (b) CD-MAO coatings.

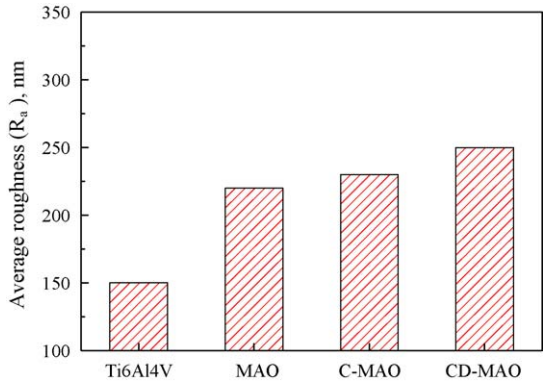

Fig. 4. The average roughness of the surfaces of the Ti6Al4V, MAO, C-MAO and CD-MAO coatings.

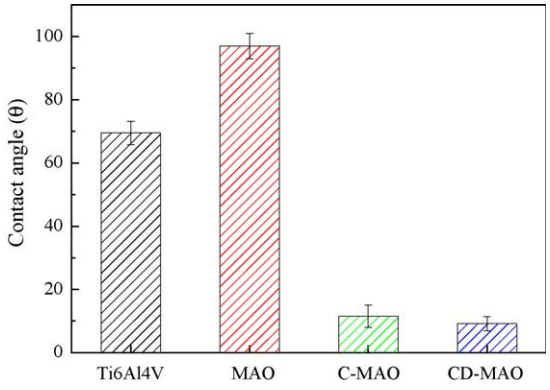

Fig. 5. The wetting angles of the distilled water droplet for Ti6Al4V, MAO, C-MAO and CD-MAO coatings.

The surface morphologies of the MAO and C-MAO coatings were discussed in the previous studies [27]. In this work, the CD-MAO coating also exhibits a surface with a network structure (Fig. 2b), similar to that of the C-MAO coating (Fig. 2a). This result indicated that subsequent heat treatment at 400 °C does not obviously alter the surface morphology of the C-MAO coating.

Fig. 3 shows the AFM images of the C-MAO and CD-MAO coatings. It was observed that the topography fluctuation of the C-MAO and CD-MAO coatings is similar. The average roughness of the MAO and C-MAO coatings is about 220 nm; that of the CD-MAO coating slightly increase to about 250 nm (Fig. 4).

Fig. 5 shows the wetting angle of the MAO coating was about 95°; while that of the C-MAO and CD-MAO coatings decreased (about 10°). This result indicated that chemical-treatment enhanced the wetting ability of the MAO coating. And subsequent dehydration did not alter the wetting property of the C-MAO coating.

Fig. 6 shows the TEM micrographs of the C-MAO and CD-MAO coatings. Nano-scale ribbon-like products with ~1 μm in length and ~100 nm in width on the surface of the C-MAO and CD-MAO coatings were observed. The electron diffraction patterns of the ribbon-like products on two coatings both show amorphous structure.

Fig. 7 shows the FT-IR spectra of the MAO, C-MAO and CD-MAO coatings. All the coatings show the presence of phosphate band at 1080–1090 cm^{-1} [30,31]. Moreover, after chemical etching, the absorption intensity of phosphate band decrease, suggesting a decrease in the P concentration of the MAO coating. Also, broad absorption peaks at 3680–2600 and 1740–1420 cm^{-1} were observed and attributed to the H_2O in the C-MAO coating [32], while no obvious broad absorption peaks of H_2O were found in the CD-MAO coating, suggesting the considerable dehydration of the C-MAO coating after heat treatment at 400 °C.

The major surface constituents found for the MAO coating are O, Ti, P, Na, Al and C according to the EDS results. However, the surfaces of the C-MAO and CD-MAO coatings show the major surface constituents of O, Ti, Na and C, as well as a few P. The P, Al and Na concentrations of the surface of the MAO coating are about 10.9, 1.9 and 2.8 at.%, and those of the surface of the CD-MAO coating are 1.3, 0.0 and 8.0 at.% (Table 2). In fact, the EDS result of the C-MAO coating already indicated the dissolution of P and Al as well

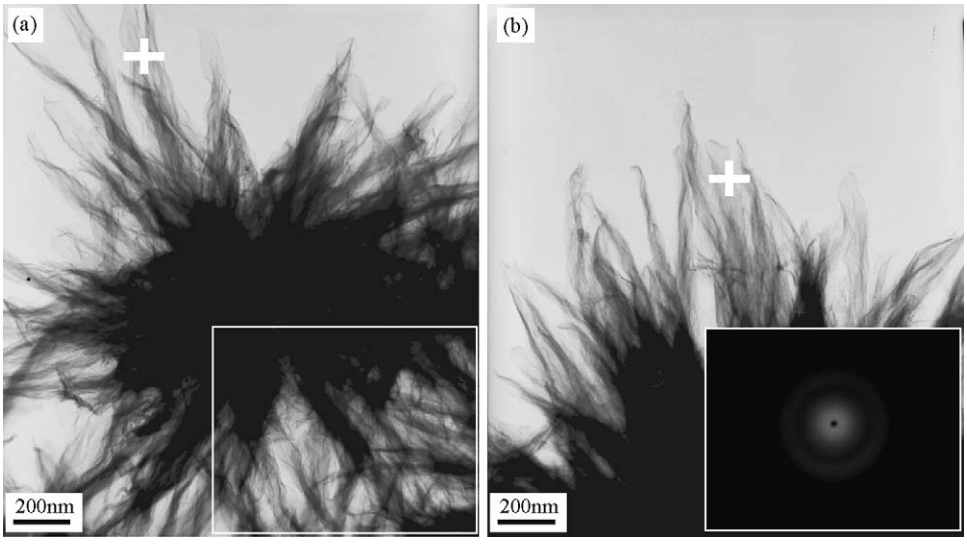

Fig. 6. TEM micrographs of (a) C-MAO and (b) CD-MAO coatings.

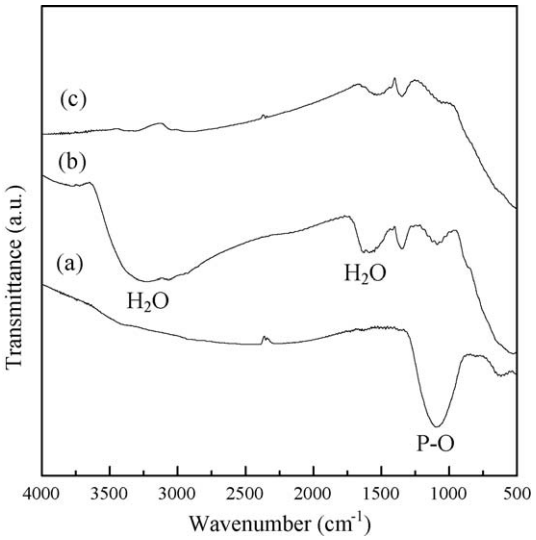

Fig. 7. FT-IR spectra of (a) MAO, (b) C-MAO and (c) CD-MAO coatings.

as the incorporation of Na during the chemical etching process (Table 2). The EDS results indicated that the surface of the CD-MAO coating is richened in O, Ti and Na similar to the C-MAO coating, suggesting that the subsequent heat treatment at 400 °C does not alter the elemental composition of the C-MAO coating.

Fig. 8 shows the XPS surveys of the surfaces of the MAO, C-MAO and CD-MAO coatings. Elements of C, Ti, O, Na and P were detected on the surface of the MAO coating, while Na

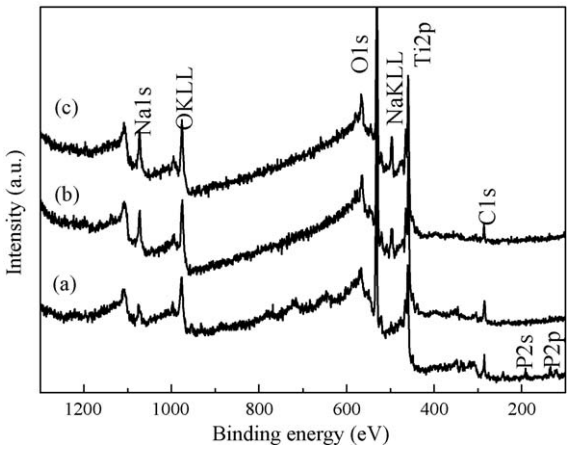

Fig. 8. XPS survey of the surfaces of (a) MAO, (b) C-MAO and (c) CD-MAO coatings.

Table 2
Elemental composition of the surfaces of the MAO coatings before and after modifications.

Element	Atomic concentration (at.%)		
	MAO	C-MAO	CD-MAO
C	6.9 ± 1.1	8.6 ± 1.5	8.0 ± 1.8
O	56.9 ± 4.5	60.1 ± 5.0	61.7 ± 6.0
Na	2.8 ± 0.8	8.4 ± 1.5	8.0 ± 1.8
P	10.9 ± 1.5	1.7 ± 0.5	1.3 ± 0.8
Ti	20.6 ± 3.0	21.2 ± 3.0	20.2 ± 4.0
Al	1.9 ± 0.5	0.0	0.0

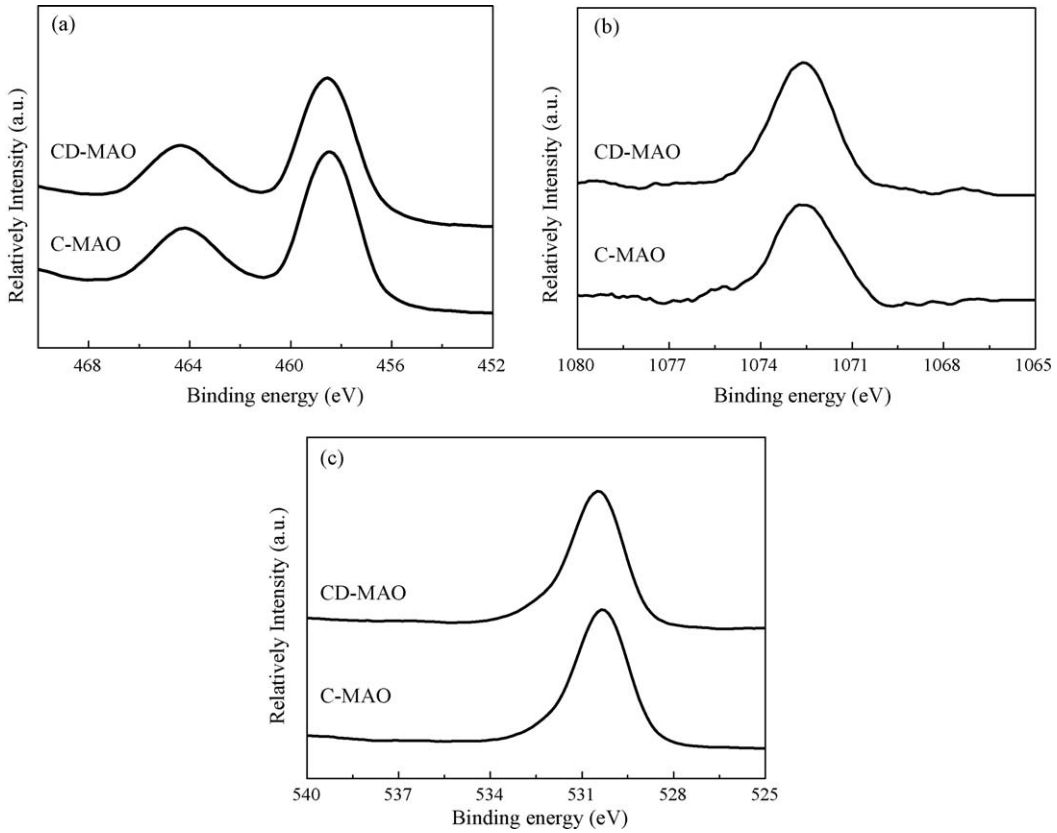

Fig. 9. Ti2p spectra of the surfaces of (a) C-MAO and (b) CD-MAO coatings.

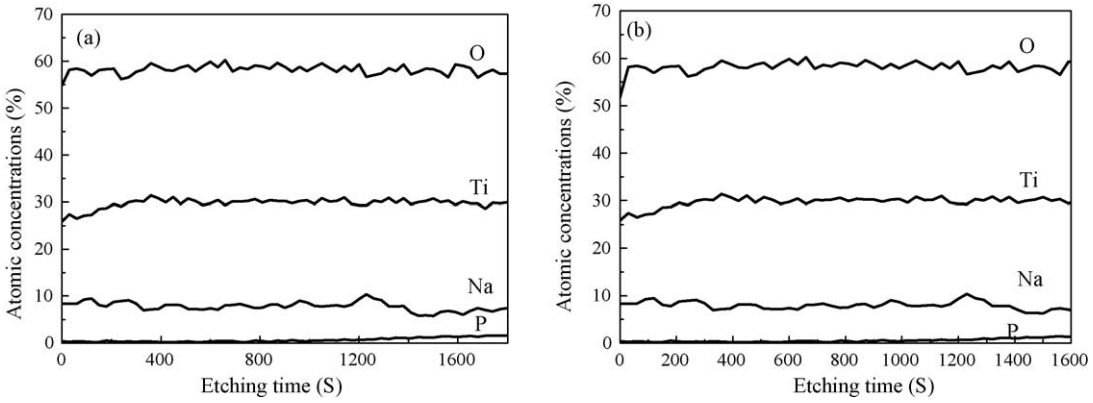

Fig. 10. AES sputtering depth profile plots near the surfaces of (a) C-MAO and (b) CD-MAO coatings.

peak increased obviously and no P was found besides Na, Ti, O and C after treatments, also suggesting the dissolution of P and introduction of Na after chemical etching, which is consistent with the EDS results. The values of the binding energies (BE) of Ti2p3/2 and Ti2p1/2 of all the coatings are 458.5 ± 0.2 and 464.4 ± 0.2 eV (Fig. 9), corresponding to a chemical state of Ti^{4+} [22,23]. The binding energies of Na1s and O1s are 1072.3 ± 0.2 and 530.4 ± 0.2 eV as shown in Fig. 9b and c, respectively, corresponding to the chemical states of Na^{+} and O^{2-}.

Fig. 10 shows AES sputtering depth profile plots near the surfaces of the C-MAO and CD-MAO coatings. The outer layers (etching time about 1200 s) of the C-MAO and CD-MAO coatings show uniform distributions in the constituents; however, only O (58–61 at.%), Ti (28–31 at.%) and Na (8–11 at.%) were detected within these layers. These results indicate that the heat treatment at 400 °C has no effect on the constituent distributions within the outer layer of the C-MAO coating.

3.2. SBF incubation of the MAO and treated MAO coatings

The surface morphologies of the C-MAO and CD-MAO coatings after SBF incubation for 7 and 14 days are shown in Fig. 11. The previous results indicated that the MAO coating did not show apatite-forming ability after SBF immersion for 7 and 14 days [27]. However, the entire surface of the C-MAO coating was covered by apatite layers after 7 and 14 days (Fig. 11a and b) [27]. In the case of the CD-MAO coating, no precipitates were found on the surface after SBF immersion for 7 days and original surface structure can still be clearly observed (Fig. 11d). After 14 days, a new layer composed of numerous sphere-like precipitates was observed on the surface of the CD-MAO coating (Fig. 11e).

In addition, at a higher magnification the surface show a network structure containing nano-scale precipitates about 100 nm in size (Fig. 11c and f). The EDS results further indicate that the new layers are composed of Ca- and P-containing (CaP) precipitates (not shown).

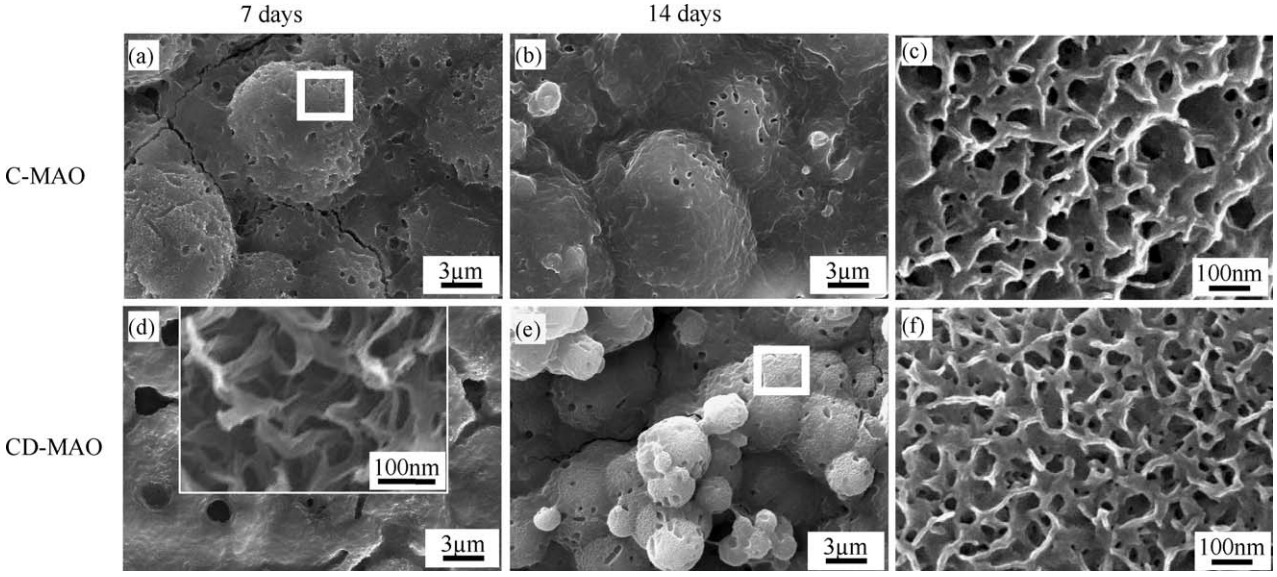

Fig. 11. Surface morphologies of the (a), (b) and (c) C-MAO, (d), (e) and (f) CD-MAO coatings after SBF incubation for 7 and 14 days; (c), (f) higher magnification of (a), (e), respectively.

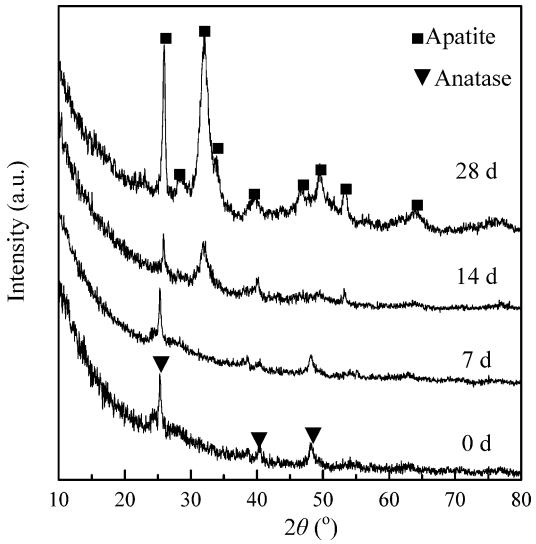

Fig. 12. XRD patterns of the CD-MAO coatings after SBF incubation for different times.

Fig. 12 shows the XRD patterns of the CD-MAO coatings before and after SBF incubation for different times. The previous result of XRD patterns of the C-MAO coating indicated that the formation of apatite after immersion for 7 days [27]. However, no changes were found on the surface of the CD-MAO coating before and after immersion for 7 days according to the XRD results (Fig. 12). After SBF incubation for 14 days, the CD-MAO coating shows the diffraction peaks of apatite with low crystallinity and the diffraction peaks of anatase and rutile disappeared completely. With increasing SBF incubation time, the diffraction peaks of apatite increase, suggesting an enhanced crystallinity. The current results indicate that subsequent dehydration greatly decreases the apatite-forming ability of the C-MAO coating.

The XPS spectra of Ca2p and P2p of the apatite formed on the C-MAO and CD-MAO coatings are shown in Fig. 13. The Ca2p spectra show a doublet at 346.8–346.9 and 350.3–350.4 eV corresponding to Ca^{2+} and P2p spectra reveals a single peak at 132.8–133.0 eV corresponding to P^{5+}. These results indicated that the subsequent dehydration of the C-MAO coating does not affect the chemical states of Ca and P in apatite

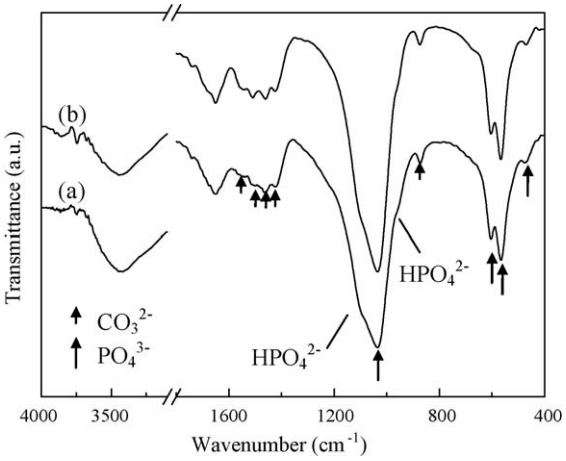

Fig. 14. FT-IR spectra of (a) C-MAO and (b) CD-MAO coatings after SBF incubation for 28 days.

induced by the substrates. In addition, these BE values are agree well with the previous results of carbonated HA obtained by biomimetic method [20].

The FT-IR spectra of the C-MAO and CD-MAO coating after SBF incubation for 28 days are similar as shown in Fig. 14. In the case of the SBF immersed CD-MAO coating, a broad absorption band at 3443 cm^{-1} and a bending mode at 1650 cm^{-1} indicate the presence of bonded water in the SBF incubated coatings [32]. The FT-IR spectrum shows absorption bands of PO_4 groups including the triply degenerated asymmetric stretching mode of $_3PO_4$ band at 1032 cm^{-1}, triply degenerated bending mode of $_4PO_4$ band at 600 and 564 cm^{-1} and double degenerated bending mode of $_2PO_4$ band at 473 cm^{-1} [31,32]. In addition, CO_3^{2-} absorption bands were observed including bending mode of $_4CO_3^{2-}$ group in A-type carbonated HA (CHA) at 1550 cm^{-1}, characteristic stretching mode of $_3CO_3^{2-}$ group in CHA at 1505 cm^{-1}, characteristic stretching mode of $_1CO_3^{2-}$ group in A-type CHA at 1462 cm^{-1}, stretching mode of $_1CO_3^{2-}$ group in B-type CHA at 1428 cm^{-1} and bending mode of ($_3$ or $_4$) CO_3^{2-} group in CHA at 874 cm^{-1} [31,32]. Also, the characteristic shoulders at 1095, 962 and 872 cm^{-1} suggest the presence of HPO_4^{2-} in the apatite. The FT-IR results confirm that the apatite formed on the two coatings has a carbonated structure.

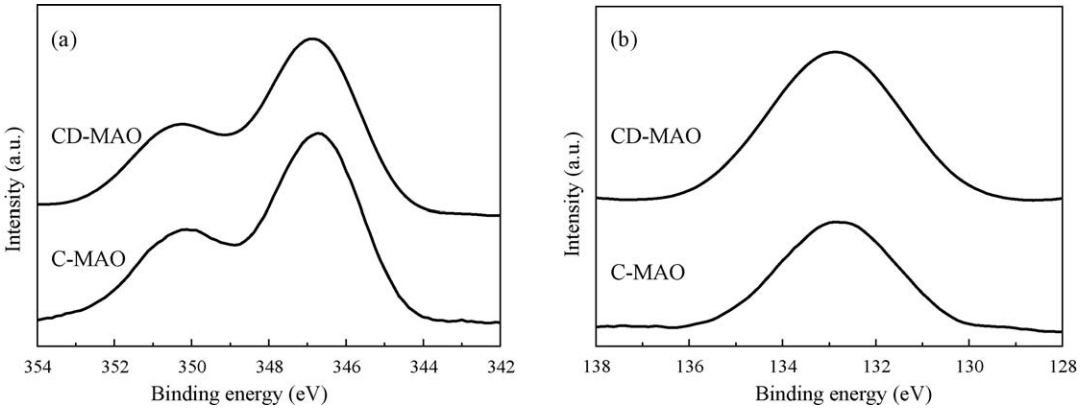

Fig. 13. XPS spectra of (a) Ca2p and (b) P2p of the apatite layer induced by the C-MAO coatings (after SBF immersion for 7 days) and CD-MAO coatings (after SBF immersion for 14 days).

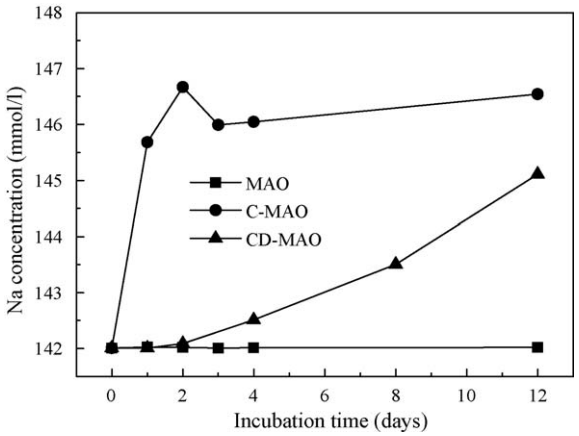

Fig. 15. Na concentrations of the SBF with immersion of all the coatings measured as a function of incubation time.

The Na concentrations of the SBF after incubation of all the coating for 0–12 days are shown in Fig. 15. It can be seen that the Na concentration of SBF with immersion of the MAO coating does not change; while those of the SBF incubation of the C-MAO and CD-MAO coatings increase during the SBF immersion process. Moreover, it is evident that the C-MAO coating is favorable for Na ions release as compared with the CD-MAO coating, indicating that the subsequent dehydration decreases the ability of Na ions release.

3.3. Cell proliferation

Fig. 16 shows the number of the MG63 cells after proliferation for 5 and 7 days on the surfaces of the control (blank slide), Ti6Al4V, MAO, C-MAO and CD-MAO coatings. Distinguish in the numbers of cell proliferation on the surfaces of control, Ti6Al4V, MAO and C-MAO films were insignificant ($p > 0.005$). Nevertheless, the CD-MAO coating is unsuitable for the cell proliferation according to the current result.

In Fig. 17, the cells spread out on the surfaces of the C-MAO and CD-MAO coatings well after culturing 3, 5 and 7 days. After 7 days, on the surfaces of the C-TOB films the cells showed smooth and flat morphology and almost contacted each other with a small gap among them, forming a continuous cell layer. In the case of the CD-MAO coating, few MG63 cells were

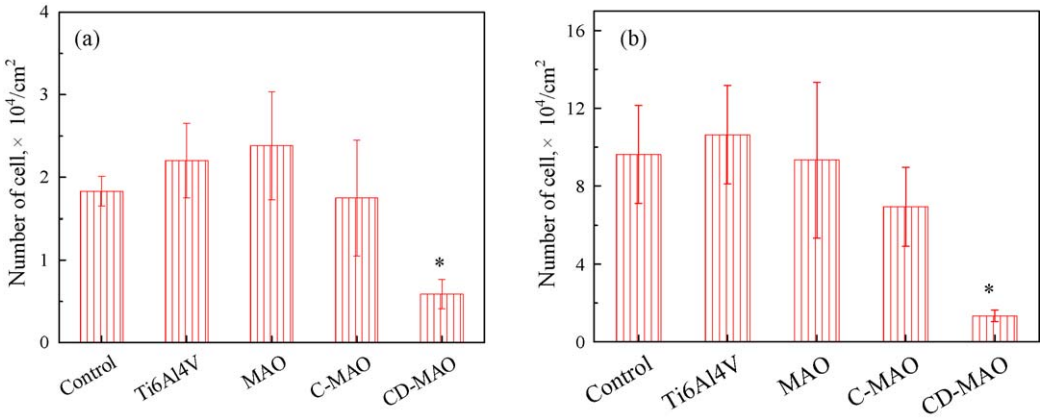

Fig. 16. Number of MG63 cells after proliferation for 5 and 7 days on the surfaces of control, Ti6Al4V, MAO, C-MAO and CD-MAO coatings: (a) 5 days and (b) 7 days. *Statistical difference $p < 0.05$ compared with the control.

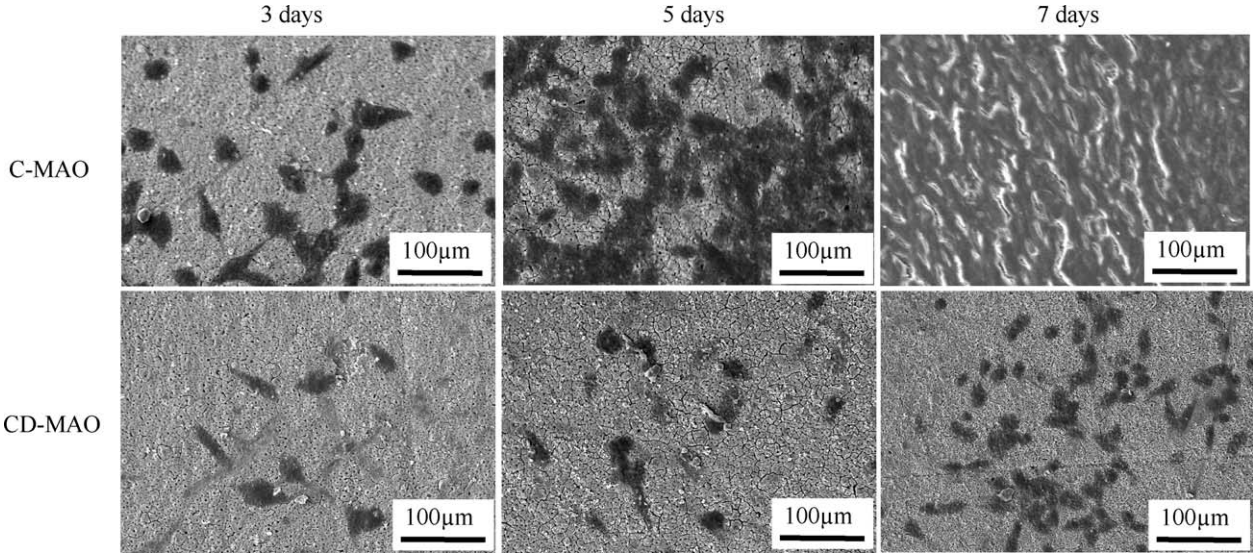

Fig. 17. SEM micrographs of the MG63 cells after culturing for 3, 5 and 7 days on the C-MAO and CD-MAO coatings.

observed its surface, not like to the C-MAO coating with a continuous cell layer.

4. Discussion

TiO_2 coating was prepared on titanium alloy by MAO technique. Specific surface structure suitable for apatite deposition was obtained by chemical etching of the surface of the MAO coating.

The XRD and SEM results indicate that the surfaces of the C-MAO and CD-MAO coatings contain anatase and amorphous phase with reticular surface morphology. The EDS and AES further indicate that the surfaces of the C-MAO and CD-MAO coatings mainly contain Na, Ti and O elements, which show a uniform distribution near the surfaces with increasing the depth. The results from the current investigation indicated that subsequent dehydration does not alter the surface constituents, surface morphology and chemical states of Ti, Na and O of the C-MAO coating.

Biomimetic apatite was successfully deposited on the surfaces of the C-MAO and CD-MAO coatings after SBF incubation for 14 days. According to the SEM, EDS and ICP-OES results, it is suggested that reactions such as ion dissolution and precipitation occur on the surfaces of the C-MAO and CD-MAO coatings during the SBF incubation process. The ICP-OES results reveal that the Na^+ ions are released from the surfaces of the C-MAO and CD-MAO coatings. According to this and previous researches [33–35], an ionic exchange between Na^+ ions of the treated MAO coatings and H_3O^+ ions of the SBF may take place during SBF incubation process. As a result, abundant Ti-OH groups are formed on the surfaces of the treated MAO coatings. The hydroxyl functionalized surfaces greatly enhance the nucleation and growth of apatite [36]. The nucleation and growth of biomimetic apatite were depicted in detail in the previous research [27,36,37]. With increasing SBF incubation time, the apatite coatings were deposited on the modified MAO coatings.

It was noted that the apatite-forming ability of the C-MAO coating decreased after dehydration. This is likely to be associated with the formation of the Ti-OH groups. It was noted that the hydrous C-MAO coating has higher ability to release Na^+ ions compared with the CD-MAO coating. The higher ability to release Na^+ ions of the hydrous C-MAO coating is probably associated with the lower energy of the related chemical bands to Na^+ ions, which needs a more thorough investigation in the future.

According to the above discussion, the decreased ability to release Na^+ ions would greatly lower the concentrations of Ti-OH groups formed by ionic exchange on the CD-MAO coating. Hence the decrease in concentrations of Ti-OH groups further leaded to a descent in apatite-forming ability of the CD-MAO coating.

For biomaterials, the surface topography, surface energy and wetting properties, etc. could affect the osteoblast adhesion and proliferation [28]. In this work, the surface roughness and wetting ability of the C-MAO and CD-MAO coatings are similar. Thus, their effect on the MG63 cell proliferation may be not obvious. Besides the above factors, chemical groups such as hydroxyl group, surface charge and surface energy, etc. could also affect the cell response [28]. In fact, the heat treatment decreased the ability of the C-MAO coating to form OH group on its surface, and altered the phase composition. On the other hand, complete dehydration take place after subsequent heat treatment. These changes could further affect the cell adhesion and proliferation, which need a more thorough investigation in the future.

5. Conclusion

The C-MAO coating exhibits high apatite-forming ability and good cell response. However, the dehydration of the C-MAO coating decreased its apatite-forming ability and MG63 cell proliferation. While subsequent dehydration does not alter on the surface morphology, major surface constituents and chemical states of Ti, Na and O of the C-MAO coating. The release of Na^+ ions from the C-MAO coating is more intensive compared with the CD-MAO coating. The weak release of Na^+ ions of the CD-MAO coating greatly decrease the formation of Ti-OH groups produced via ionic exchange between Na^+ and H_3O^+ ions in SBF. Thus it further decreased the induction capability for apatite formation of the CD-MAO coating.

Acknowledgement

This work was financially supported by National Natural Science Foundation of China (Grant No. 50872025).

References

[1] M. Wang, Developing bioactive composite materials for tissue replacement, Biomaterials 24 (2003) 2133–2151.
[2] L.L. Hench, Bioceramics, J. Am. Ceram. Soc. 81 (7) (1998) 1705–1728.
[3] J.M. Gomez-Vega, E. Saiz, A.P. Tomsia, T. Oku, K. Suganuma, G.W. Marshall, S.J. Marshall, Novel bioactive functionally graded coatings on Ti6Al4V, Adv. Mater. 12 (2000) 894–899.
[4] C.Q. Ning, Y. Zhou, In vitro bioactivity of a biocomposite fabricated from HA and Ti powders by powder metallurgy method, Biomaterials 23 (2002) 2909–2915.
[5] Y.C. Yang, E.W. Chang, B.H. Hwang, S.Y. Lee, Biaxial residual stress states of plasma-sprayed hydroxyapatite coatings on titanium alloy substrate, Biomaterials 21 (2000) 1327–1337.
[6] C.F. Feng, K.A. Khor, E.J. Liu, P. Cheang, Phase transformations in plasma sprayed hydroxyapatite coatings, Scripta Mater. 42 (2000) 103–109.
[7] X.B. Zheng, M.H. Huang, C.X. Ding, Bond strength of plasma-sprayed hydroxyapatite/Ti composite coatings, Biomaterials 21 (2000) 841–849.
[8] M.F. Hsieh, L.H. Perng, T.S. Chin, Hydroxyapatite coating on Ti6Al4V alloy using a sol–gel derived precursor, Mater. Chem. Phys. 74 (2002) 245–250.
[9] E. Milella, F. Cosentino, A. Licciulli, C. Massaro, Preparation and characterisation of titania/hydroxyapatite composite coatings obtained by sol–gel process, Biomaterials 22 (2001) 1425–1431.
[10] A.E. Porter, P. Taak, L.W. Hobbs, M.J. Coathup, G.W. Blunn, M. Spector, Bone bonding to hydroxyapatite and titanium surfaces on femoral stems retrieved from human subjects at autopsy, Biomaterials 25 (2004) 5199–5208.
[11] Y.C. Yang, E. Chang, Influence of residual stress on bonding strength and fracture of plasma-sprayed hydroxyapatite coatings on Ti6Al4V substrate, Biomaterials 22 (2001) 1827–1836.

[12] B.C. Yang, M. Uchida, H.M. Kim, X.D. Zhang, T. Kokubo, Preparation of bioactive titanium metal via anodic oxidation treatment, Biomaterials 25 (2004) 1003–1010.
[13] H.W. Kim, Y.H. Koh, L.H. Li, S. Lee, H.E. Kim, Hydroxyapatite coating on titanium substrate with titania buffer layer processed by sol–gel method, Biomaterials 25 (2004) 2533–2538.
[14] A.L. Yerokhin, X. Nie, A. Leyland, A. Matthews, S.J. Dowey, Plasma electrolysis for surface engineering, Surf. Coat. Technol. 122 (1999) 73–93.
[15] X. Nie, A. Leyland, A. Matthews, Deposition of layered bioceramic hydroxyapatite/tio$_2$ coatings on titanium alloys using a hybrid technique of microarc oxidation and electrophoresis, Surf. Coat. Technol. 125 (2000) 407–414.
[16] Y. Han, S.H. Hong, K.W. Xu, Structure and in vitro bioactivity of titania-based films by micro-arc oxidation, Surf. Coat. Technol. 168 (2003) 249–258.
[17] L.H. Li, Y.M. Kong, H.W. Kim, Improved biological performance of Ti implants due to surface modification by micro-arc oxidation, Biomaterials 25 (2004) 2867–2875.
[18] X.L. Zhu, K.H. Kim, Y.S. Jeong, Anodic oxide films containing Ca and P of titanium biomaterial, Biomaterials 22 (2001) 2199–2206.
[19] X.L. Zhu, L.O. Joo, S.Y. Kim, K.H. Kim, Surface characteristics and structure of anodic oxide films containing Ca and P on a titanium implant material, J. Biomed. Mater. Res. 60 (2002) 333–338.
[20] W.H. Song, Y.K. Jun, Y. Han, Biomimetic apatite coatings on microarc oxidized titania, Biomaterials 25 (2004) 3341–3349.
[21] J.Z. Chen, Y.L. Shi, L. Wang, F.Y. Yan, F.Q. Zhang, Preparation and properties of hydroxyapatite-containing titania coating by micro-arc oxidation, Mater. Lett. 60 (2006) 2538–2543.
[22] V.M. Frauchiger, F. Schlottig, B. Gasser, M. Textor, Anodic plasma-chemical treatment of CP titanium surfaces for biomedical applications, Biomaterials 25 (2004) 593–606.
[23] J.P. Schreckenbach, G. Marx, F. Schlottig, M. Textor, N.D. Spencer, Characterization of anodic spark-converted titanium surfaces for biomedical applications, J. Mater. Sci.: Mater. Med. 10 (1999) 453–457.
[24] D.Q. Wei, Y. Zhou, Y.M. Wang, D.C. Jia, Characteristic of microarc oxidized coatings on titanium alloy formed in electrolytes containing chelate complex and nano-HA, Appl. Surf. Sci. 253 (2007) 5045–5050.
[25] W.H. Song, H.S. Ryu, S.H. Hong, Apatite induction on Ca-containing titania formed by micro-arc oxidation, J. Am. Ceram. Soc. 88 (2005) 2642–2644.
[26] L.H. Li, H.W. Kim, S.H. Lee, Y.M. Kong, H.E. Kim, Biocompatibility of titanium implants modified by microarc oxidation and hydroxyapatite coating, J. Biomed. Mater. Res. A 73 (2005) 48–54.
[27] D.Q. Wei, Y. Zhou, Y.M. Wang, D.C. Jia, Chemical etching of micro-plasma oxidized titania film on titanium alloy and apatite deposited on the surface of modified titania film in vitro, Thin Solid Films 516 (2008) 1818–1825.
[28] M. Uchida, H.M. Kim, T. Kokubo, S. Fujibayashi, T. Nakamura, Structural dependence of apatite formation on titania gels in a simulated body fluid, J. Biomed. Mater. Res. A 64 (2003) 164–170.
[29] A. Oyane, H.M. Kim, T. Furuya, T. Kokubo, T. Miyazaki, T. Nakamura, Preparation and assessment of revised simulated body fluids, J. Biomed. Mater. Res. A 65 (2003) 188–195.
[30] D.M. Liu, Q.Z. Yang, T. Troczynski, Sol–gel hydroxyapatite coatings on stainless steel substrates, Biomaterials 23 (2002) 691–698.
[31] S. Koutsopoulos, Synthesis and characterization of hydroxyapatite crystals: a review study on the analytical methods, J. Biomed. Mater. Res. 62 (2002) 600–612.
[32] L. Müller, F.A. Müller, Preparation of SBF with different HCO_3^- content and its influence on the composition of biomimetic apatites, Acta Biomater. 2 (2006) 181–189.
[33] H.M. Kim, F. Miyaji, T. Kokubo, T. Nakamura, Preparation of bioactive Ti and its alloys via simple chemical surface treatment, J. Biomed. Mater. Res. 32 (1996) 409–417.
[34] H.M. Kim, F. Miyaji, T. Kokubo, S. Nishiguchi, T. Nakamura, Graded surface structure of bioactive titanium prepared by chemical treatment, J. Biomed. Mater. Res. 45 (1999) 100–107.
[35] H. Takadama, H.M. Kim, T. Kokubo, T. Nakamura, An X-ray photoelectron spectroscopy study of the process of apatite formation on bioactive titanium metal, J. Biomed. Mater. Res. 55 (2001) 185–193.
[36] G.K. Toworfe, R.J. Composto, I.M. Shapiro, P. Ducheyne, Nucleation and growth of calcium phosphate on amine-, carboxyl- and hydroxyl-silane self-assembled monolayers, Biomaterials 27 (2006) 631–642.
[37] C.B. Mao, H.D. Li, F.Z. Cui, Q.L. Feng, C.L. Ma, The functionalization of titanium with EDTA to induce biomimetic mineralization of hydroxyapatite, J. Mater. Chem. 9 (1999) 2573–2582.